

The time-resolved stereoscopic digital particle image velocimetry up to 26.7 kHz

by

M. Tanahashi⁽¹⁾, Y. Fukuchi⁽¹⁾, G.-M. Choi⁽²⁾, K. Fukuzato⁽³⁾ and T. Miyauchi⁽¹⁾

⁽¹⁾Department of Mechanical and Aerospace Engineering, Tokyo Institute of Technology
2-12-1 Ookayama, Meguro-ku, Tokyo 152-8552, Japan
E-Mail: mtanahas@mes.titech.ac.jp

⁽²⁾School of Mechanical Engineering, Pusan National University
30 Jangjeon-dong, Geumjeong-gu, Busan 609-735, Korea

⁽³⁾Strategic Business Planning Administration, Seika Corporation
3F Shin Tokyo Bldg. 3-3-1 Marunouchi Chiyoda-ku, Tokyo 100-0005, Japan

ABSTRACT

A time-resolved stereoscopic digital PIV system has been developed with high-repetition-rate Nd:YAG lasers for industrial processing and high-speed CMOS cameras. The developed system was applied to the velocity measurement of a turbulent jet and a swirl-stabilized combustor. It is shown that velocity measurement up to 26.7kHz is possible and the results represent dynamics of the turbulence structure very well as shown in Fig. 1 (a). Accuracy of several PIV algorithms such as a spatial-temporal filter method (Tanahashi et al. 2003), a 2-step hierarchical method (Kumar and Banerjee 1995) and a window-offset method (Westerweel et al. 1997) have shown for the time-resolved measurement. Figure 1 (b) shows power spectrums of the three velocity components obtained by the time-resolved stereoscopic PIV in a turbulent swirling flow. The time-resolved stereoscopic PIV can provides energy spectrums of three velocity components as well as the time-averaged feature of the turbulent flows with high accuracy. This system is potentially applicable from several hundred Hz to several tens kHz, and would contribute to developments of the turbulence research in the near future.

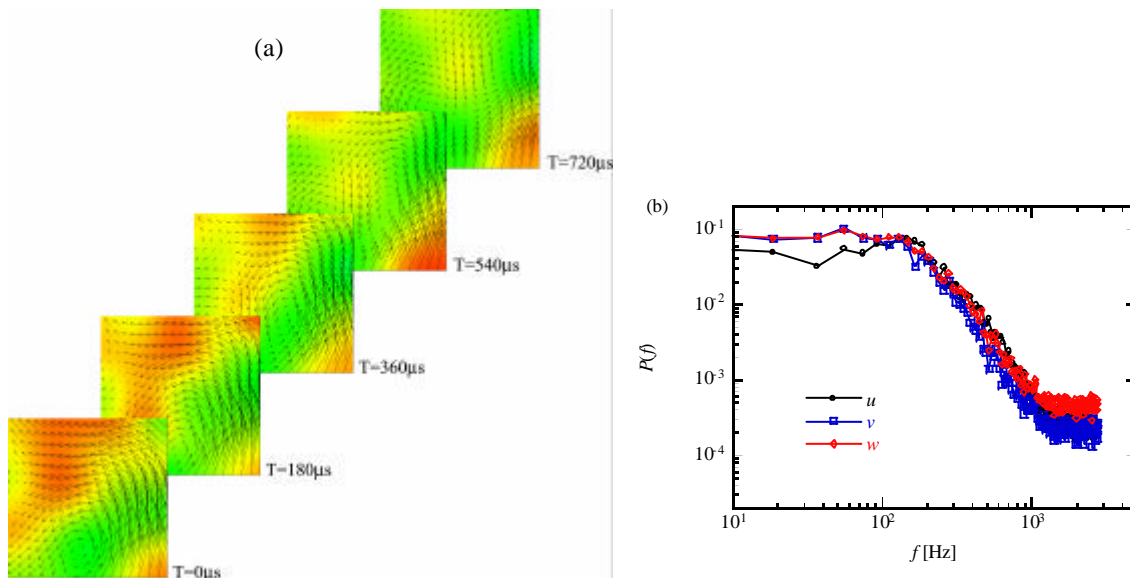


Fig. 1. Time resolved stereoscopic digital PIV results.

- (a) Time-series vector maps of turbulent swirling flows. Velocity magnitude across the measurement plane is shaded and shown with velocity vector in the measurement plane. The velocity from behind the sheet to the front has positive value and is denoted by red color.
- (b) Power spectrums of the three velocity components obtained by the time-resolved stereoscopic PIV in a turbulent swirling flow.

1. INTRODUCTION

Particle image velocimetry (PIV), which gives instantaneous field maps of the velocity components, is an useful, firmly established, non-intrusive measurement technique in fluid flow (Dudderrar and Simpkins 1977, Keane and Adrian 1990, Adrian 1991). To apply this PIV measurement to various industrial purposes as well as fundamental research, many research groups have explored extensively over the past decade. The use of a CCD camera for imaging the flow provides one method to construct a real-time PIV system (Willert and Gharib 1991, Schmidt and Loffler 1993). In addition, optical correlation processing method has been explored to reduce the time of PIV transparencies (Sharpe and Johnson 1992, Mao et al. 1993). The accuracy and precision of digital PIV measurements were investigated experimentally for a range of various parameters such as seeding density and focusing (Megerle et al. 2002). For measurements of three velocity components of flow fields, a number of techniques have been proposed such as stereoscopic (Arroyo and Greated 1991, Grant et al. 1995, Lawson and Wu 1997, Zang and Prasad 1997, Gaydon et al. 1997), holographic (Coupland and Halliwell 1992) and dual-plane three-dimensional PIV (Raffel et al. 1995, Bruecker 1996, Schlicke and Greated 2002). However, these conventional PIVs have relatively low temporal resolutions, which are up to several tens Hz for enough spatial resolution, because spatial and temporal resolutions are trade-off in PIV. To investigate temporal developments of turbulent flows, high temporal resolution has been required as well as the spatial resolution.

The combining of PIV (close to PTV) and high speed photography was conducted to track a unsteady fluid flow (Vogel and Lauterborn 1988), but the use of the light scattering in the forward direction limited the spatial resolution. To record the time evolution of the gas velocity field and the flame boundary, a cinema PIV technique was used for turbulent combustion (Upatnieks et al. 2002). Image reproduction from movie camera to CCD camera is necessary to obtain vector maps for this cinema PIV. Recently, high-speed acquisition with several hundreds Hz PIV measurements became possible with a development of high speed CCD and CMOS cameras (Tanahashi et al. 2002a, Ibsen et al. 2003, Sung and Yoo 2003). To investigate turbulence characteristics in detail, however, more high spatial and temporal resolution up to several tens kHz is required. Especially, to understand the dynamics of vortical structure and its relations with turbulence statistics, sequence images of eddy motions with high temporal resolution are helpful. In our previous study, we have developed a time-resolved two dimensional PIV up to 8kHz (Tanahashi et al. 2003).

In this study, a time-resolved stereoscopic digital PIV system up to several tens kHz with high spatial resolution has been developed by using CMOS high-speed cameras and two high-repetition-rate pulse lasers, and availability and potential of this time-resolved stereoscopic PIV system are shown through the measurements in turbulent jets and turbulent swirling flows in a swirl-stabilized combustor without combustion.

2. TIME-RESOLVED STEREOSCOPIC PIV

Figure 1 shows a schematic of the time-resolved stereoscopic digital PIV system developed in this study. This system consists of two Nd:YAG lasers, optical system, two CMOS cameras (Vision Research, Phantom V5.0 or V7.0) and a pulse generator (LabSmith, LC880). The frequency of Nd:YAG lasers in conventional PIV is no more than several tens Hz. In this study, we have adopted high power and high-repetition-rate pulse lasers for industrial processing as a light source. The maximum power of these lasers is 50W at 10kHz. Laser beams from two lasers become double-pulsed beams through the laser beam combining optics, and the double-pulsed beams are expanded by the laser sheet optics. Here, to combine two laser beams, a polarizer and a half-wave plate are used. The double-pulsed laser sheets illuminate the measurement region and scattered light by tracer particles is recorded by the high-speed CMOS cameras. The thickness of the laser sheet is about 380 μ m. The CMOS camera used in this study can record images with 1024 \times 1024 pixels at 1000 frames/s (512 \times 512 pixels at 3700 frames/s) or 800 \times 600 pixels at 4800 frames/s (512 \times 512 pixels at about 8300frames/s). The CMOS cameras are located with ± 18 degree inclined for normal to the measurement plane to capture stereoscopic particle images.

The CMOS camera starts to expose 3 μ s after the trigger negative edge. Beams from each laser are synchronized to each frame interval. Repetition rates of two Nd:YAG lasers are a half of the camera frame rate respectively and velocity vectors are calculated from successive images by a cross correlation method. Generally, cameras need the dead time (T_s) to store data between camera frames and the time interval of successive images (Δt) is limited by this dead time. The theoretical minimum T_s of the CMOS camera used in this study is about 5 μ s. The images can be acquired with $\Delta t = 7\mu$ s in our preliminary tests, which means that this PIV system can be applicable to relatively high-speed flows.

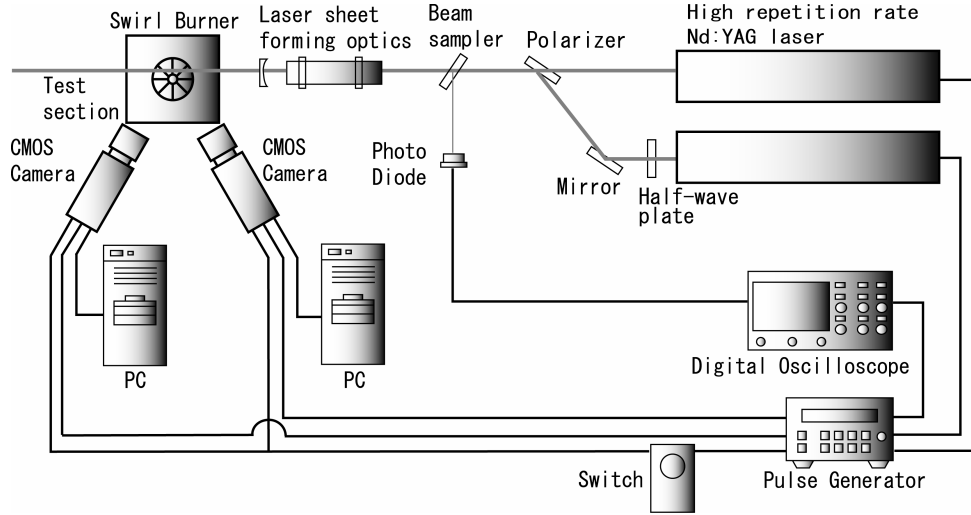


Fig. 1. Schematic of the time-resolved stereoscopic digital PIV.

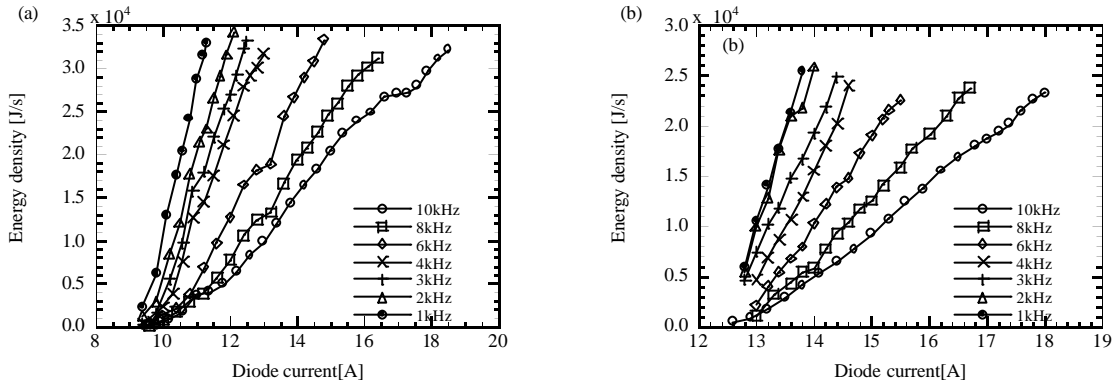


Fig. 2. Relationship between laser current and energy density of the laser pulse. (a) laser-1, (b) laser-2.

For the measurements with several tens kHz frame rates, high power laser is required to take sharp particle images. Figure 2 shows the relation between current to the pump diode and energy density of the laser pulse for each laser used in this study. For a constant current to the pump diode, the energy density of the laser pulse increases with the decrease of the repetition frequency. To prevent damages of laser, the energy density should be kept to lower than that of the maximum power condition: 50W at 10kHz. The lowest repetition frequency of the present lasers is about 1kHz and the highest one is more than 20kHz. These correspond to the frequency range of the present PIV system. For the case of lower frequency, CW-laser is enough to get particle images. Using CW-laser such as Ar⁺ laser with 4W instead of two Nd:YAG lasers, 3969 velocity vectors at 300Hz was successfully obtained in water flows (Tanahashi et al. 2002a).

In this study, high spatial resolution PIV algorithm developed by our previous study (Tanahashi et al. 2002b) is used. In the turbulent free shear flow, because mean velocity changes across the measurement region, particle displacements are different for each interrogation region. Therefore, we have tested a 2-step hierarchical method (Kumar and Banerjee 1995) and a window offset method (Westerweel et al. 1997). Furthermore, to ensure the accuracy of the PIV measurement, the elimination scheme of the spurious vectors and noises is established by a PIV simulation based on DNS of particle-laden homogeneous isotropic turbulence. Note that number of the spurious vectors included in the raw data is very few (less than 0.5%) in the present measurements and the elimination scheme is mainly used to cutoff the high wave number noises which exceed the spatial resolution of PIV. The high wave number noises are introduced by the overlap of the interrogation regions. From two-dimensional velocity fields obtained by each CMOS camera, three component velocity vectors on a two-dimensional plane are calculated by using a geometrical relation (Arroyo and Greated 1991, Westerweel and Nieuwstadt 1991, Willert 1997, Prasad 2000). As spurious vectors can not be completely eliminated by instantaneous velocity vectors, temporal low pass filter, which is one advantage of the present time-resolved PIV, was also adopted in the present work.

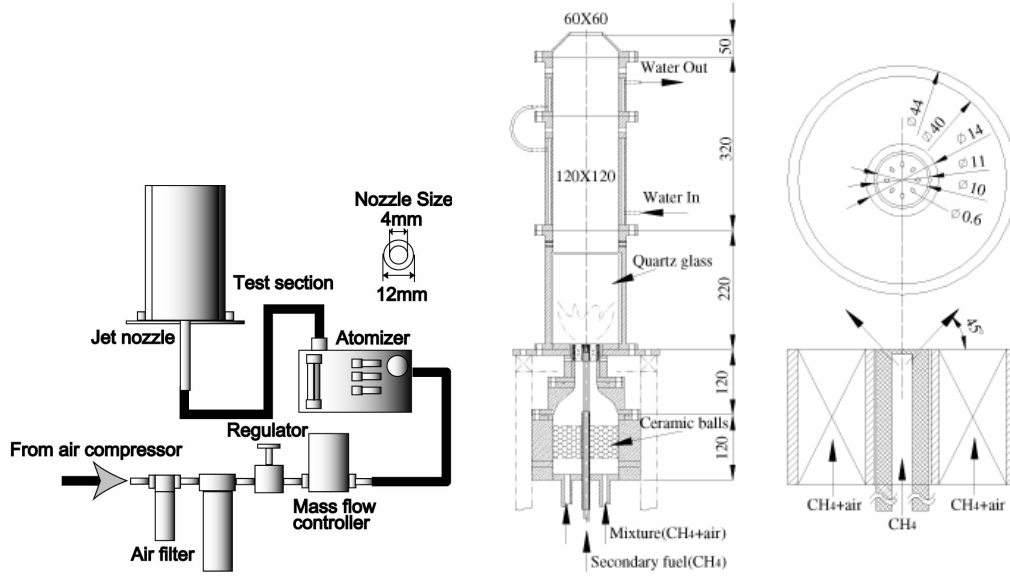


Fig. 4. Experimental apparatus of a turbulent jet (left) and a swirl-stabilized combustor (right).

Table 1. Experimental conditions in turbulent jets. Re_D : Reynolds number based on the mean exit velocity and nozzle diameter, x : distance from the jet exit, L_i : the length of measurement region in the i th direction, Rc_i : CMOS camera resolution in the i th direction, f_c : frame rate of the CMOS camera, f_l : frequency of the Nd:YAG lasers, P_l : total power of the lasers and Δt : time interval between successive particle images.

	Case 1	Case 2	Case 3	Case 4
Re_D	5316	5316	3824	3824
x/D	60	60	15	15
$L_x \times L_y$ [mm]	15.4 × 15.4	10.6 × 10.6	7.68 × 7.68	6.80 × 6.80
$Rc_x \times Rc_y$ [pixels]	512 × 512	352 × 352	256 × 256	256 × 256
f_c [kHz]	6.0	16.0	26.7	26.7
f_l [kHz]	6.0	16.0	26.7	13.35
P_l [W]	23.4	42	42	82
Δt [ms]	166.7	62.5	37.5	15

3. VELOCITY MEASUREMENTS IN TURBULENCE

3.1 Experimental Apparatus of a Turbulent Jet and a Swirl-Stabilized Combustor

Figure 4 shows the experimental apparatus of a turbulent jet and swirl-stabilized combustor. In the case of the turbulent jet, air from a compressor is regulated to a constant pressure and constant flow rate by pressure regulators and a digital mass flow controller, and is seeded with droplets generated by an atomizer (TSI, Six-Jet Atomizer, Model 9306). Then the air is led to a nozzle to form a jet. In this study, DOS (dioctyl sebacate) was used as tracer particles. The external and internal diameters of the nozzle are 12mm and 4mm, respectively. To prevent spreading of particles to circumference, the test section is surrounded by an acrylic duct with cross section area of 32cm × 32cm. In this study, measurement was carried out for $Re_D=3284$ and 5316, where Re_D is Reynolds number based on the nozzle diameter and mean axial velocity at the jet exit.

As for the swirl-stabilized combustor, the combustion rig consists of a contraction section, a swirl nozzle section and combustion chamber. On each side of combustion chamber, a silica glass plate was installed to allow optical access. The swirl nozzle has swirl vanes of 14mm inner diameter and 40mm outer diameter, inclined 45 degree from the nozzle axis. Although a secondary fuel nozzle was mounted at center of the swirl vanes, this nozzle was not used in the present study. The measurements by the time-resolved stereoscopic PIV are conducted for inert flows in this

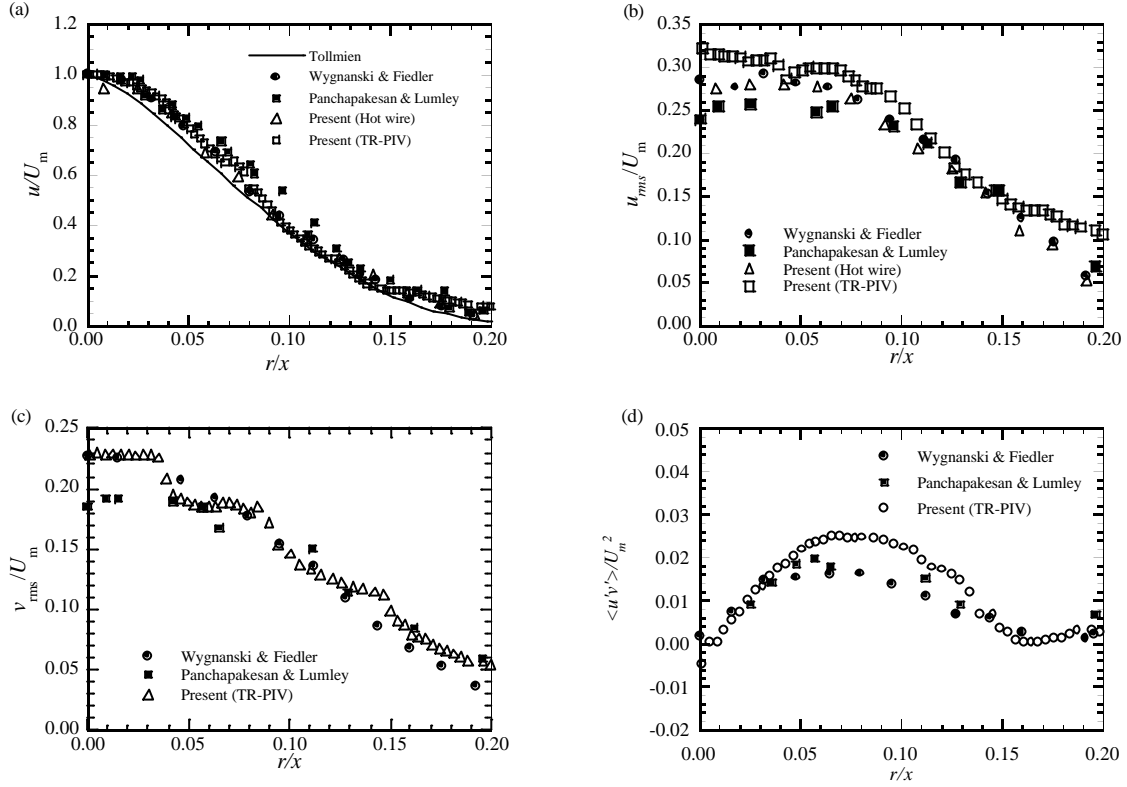


Fig. 4. Mean axial velocity (a), axial velocity fluctuation (b), radial velocity fluctuation(c) and Reynolds stress (d) across the jet.

combustor. As for the tracer particles, $5\mu\text{m SiO}_2$, $0.4\mu\text{m TiO}_2$ and $0.18\mu\text{m Al}_2\text{O}_3$ were tested, and then SiO_2 are used for tracer particles in this study.

3.2 Two-Dimensional Time-Resolved PIV Measurements in Turbulent Jets

In this study, conventional two-dimensional measurements were conducted in turbulent jets to show the potential of this time-resolved PIV system. Table 1 shows experimental conditions in turbulent jets. Measurements were conducted for four different conditions. Case 1 and Case 2 were conducted at $x/D=60$ where mean velocity is about 2.0m/s. For these cases, since the laser and camera frequency is enough to capture the turbulent motions, equally spaced laser pulses by a single laser are used. To investigate effects of PIV algorithms such as a 2-step hierarchical method (Kumar and Banerjee 1995) and a window-offset method (Westerweel et al. 1997), spatial resolutions of these cases is selected to be equal ($30\mu\text{m}$). In Case 3 and Case 4, the maximum performance of the present time-resolved PIV is exploited near the exit of the jets. The final interrogation region for Case 1 is selected to be 24×24 pixels with the first interrogation region of 48×48 pixels and effects of the 2-step hierarchical method are examined. In Case 2, effectiveness of the window offset method is investigated by using a single interrogation region of 24×24 pixels.

The statistical properties such as the mean axial velocity, axial velocity fluctuation, radial velocity fluctuation and Reynolds stress have been compared with a hot-wire measurement conducted in the present work, a theoretical work (Tollmien 1926) and the previous results by Wygnanski and Fiedler (1969) and Panchapakesan and Lumley (1993). Figure 4 shows mean axial velocity, axial velocity fluctuation, radial velocity fluctuation and Reynolds stress. All profiles measured by the present PIV is close to other results within small discrepancy. These results indicate that the time-resolved PIV represents the typical characteristics of the turbulent jet with high accuracy.

Figure 5 shows power spectrums of the streamwise velocity component measured by the present time-resolved PIV with 6kHz and 16kHz for $Re_D=5316$ and $x/D=60$. The power spectrum measured by a x-probe hotwire at the same point is also plotted for comparison. The power spectrum obtained by the hotwire shows a traditional turbulence characteristics in the overall frequency ranges. Especially, the power spectrum obtained by the hotwire shows $-5/3$

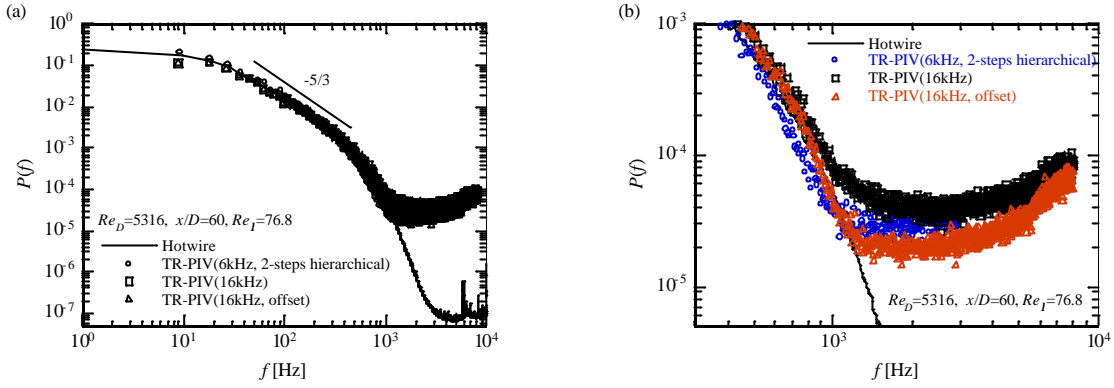


Fig. 5. Power spectrums of the streamwise velocity component measured by time-resolved PIV and hotwire. (a) All frequency region, (b) high frequency region.

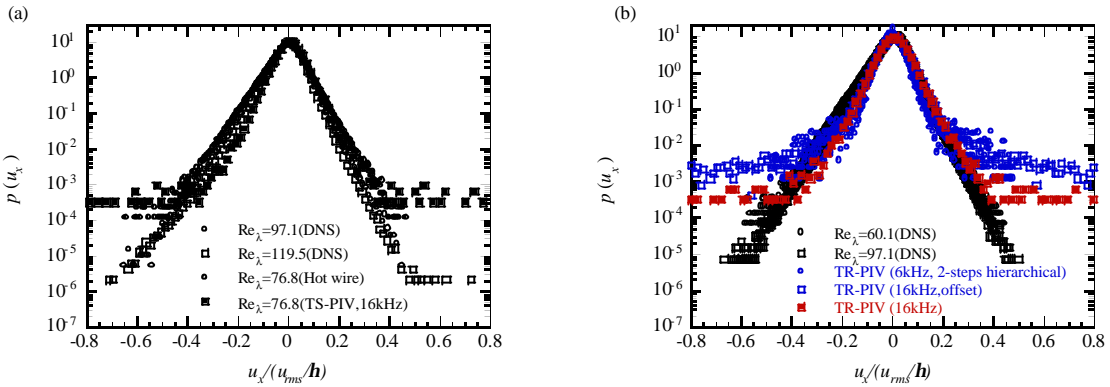


Fig. 6. Probability density functions of longitudinal velocity derivatives of axial velocity. (a): results of the time resolved PIV with DNS and a hot wire, (b): effects of PIV algorithms.

power law from 100 Hz to 500 Hz region, which indicates that the flow reaches fully developed turbulent state. The power spectrum by the time-resolved PIV also show $-5/3$ power law region in the inertial subrange, which indicates that the present time-resolved PIV can measure temporal evolution of turbulent flows which have distinct inertial subrange. The power spectrum by the time-resolved PIV becomes flat in the dissipation range compared with that by the hotwire. This behavior is caused by the effective frequency limit due to the interrogation. Measurable maximum frequency for the first and second interrogation can be approximately estimated as 1.39kHz and 2.77kHz, respectively. These frequencies are calculated based on the mean streamwise velocity and spatial resolution. The frequency where the energy becomes a constant value in Fig. 5 (a) corresponds to the maximum frequency of the first interrogation. In Fig. 5 (b), energy spectrums in high frequency regions are magnified. The window-offset method by Westerweel et al. (1997) improves over estimations of turbulence energy in the high frequency region. On the other hand, the hierarchical method proposed by Kumar and Banerjee (1995) gives under estimations of the energy in the high frequency region. This fact suggests that the hierarchical method is not always effective in the time-series measurements.

Probability density function of streamwise derivative of axial velocity are shown in Fig. 6 for $Re_D=5316$ and $x/D=60$. The probability density functions of the velocity derivatives obtained by the time-resolved PIV without the hierarchical method and the window offset method shows good agreement with those by DNS and hotwire measurement. However, Fig. 6 (b) shows that the use of the hierarchical method and the window offset method work worth to get proper velocity derivatives. As shown in the above, the window offset method gives improvements in the energy spectrum in high frequency region, whereas the derivative information are contaminated by the window offset. To estimate the performance of the present time-resolved PIV, turbulence statistics, that is, Kolmogorov microscale h and Reynolds number based on Taylor microscale Re_l , were estimated by adopting Taylor's hypothesis. The measured h and Re_l by the time-series PIV were 1.29×10^{-4} m and 76.1, respectively. These values are somewhat larger than results by hotwire with 5.6% for h and 0.98% for Re_l . As these measurement errors are also tolerable, we could investigate the dynamics of vortical structure with high spatial resolution. The movie of the turbulent flow obtained for 26.7kHz shows dynamics of the vortical structures very well. Turbulence statistics can provide useful information for

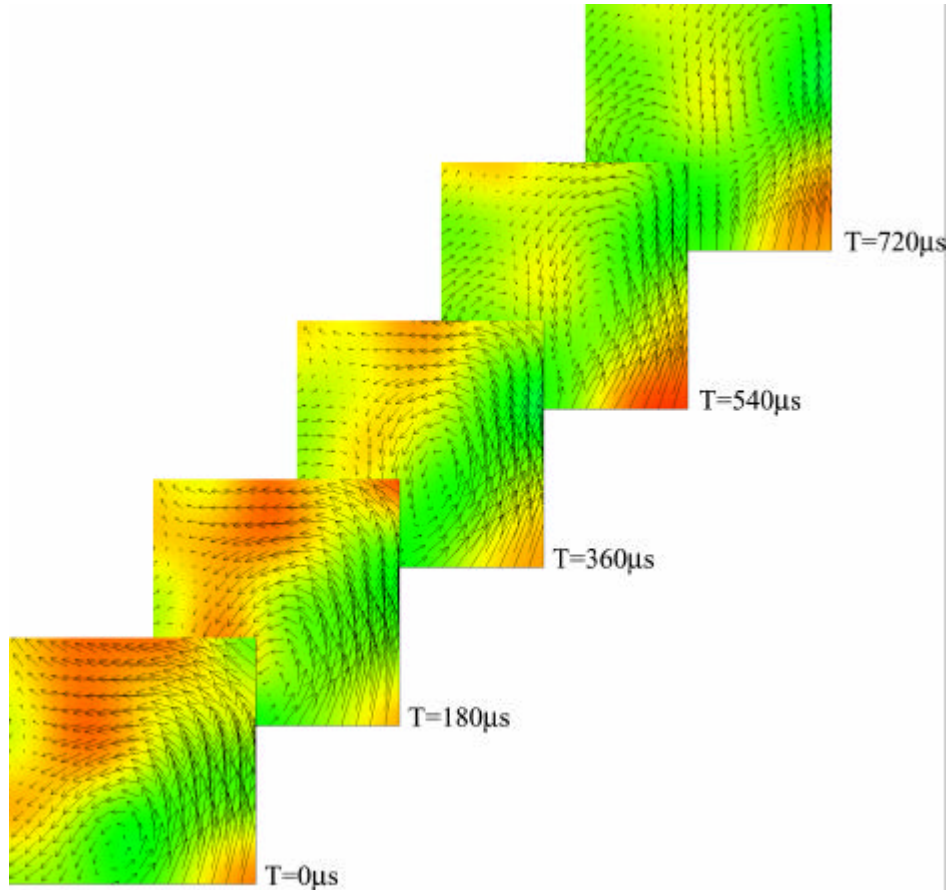


Fig. 7. Time-series vector maps of turbulent swirling flows. Velocity magnitude across the measurement plane is shaded and shown with velocity vector in the measurement plane. The velocity from behind the sheet to the front has positive value and is denoted by red color.

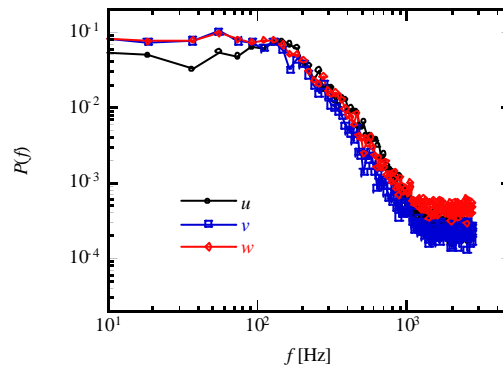


Fig. 8. Power spectrums of the three velocity components obtained by the time-resolved stereoscopic digital PIV in turbulent swirling flows.

understandings the turbulent structures in detail (Tanahashi et al. 2003).

3.2 Time-Resolved Stereoscopic PIV Measurements in Turbulent Swirling Flows

Based on the two-dimensional measurements in the previous section, the PIV system is extended for the time-resolved stereoscopic PIV. The time-resolved stereoscopic PIV was applied for inert turbulent swirling flows in the swirl-stabilized combustor shown in Fig. 4. Figure 7 shows time-series vector maps of turbulent swirling flows. This measurement is conducted with 11.1kHz, 256×256 pixels and $\mathbf{Dt} = 30\mu\text{s}$ for $4.4\text{mm} \times 4.4\text{mm}$ region. Velocity

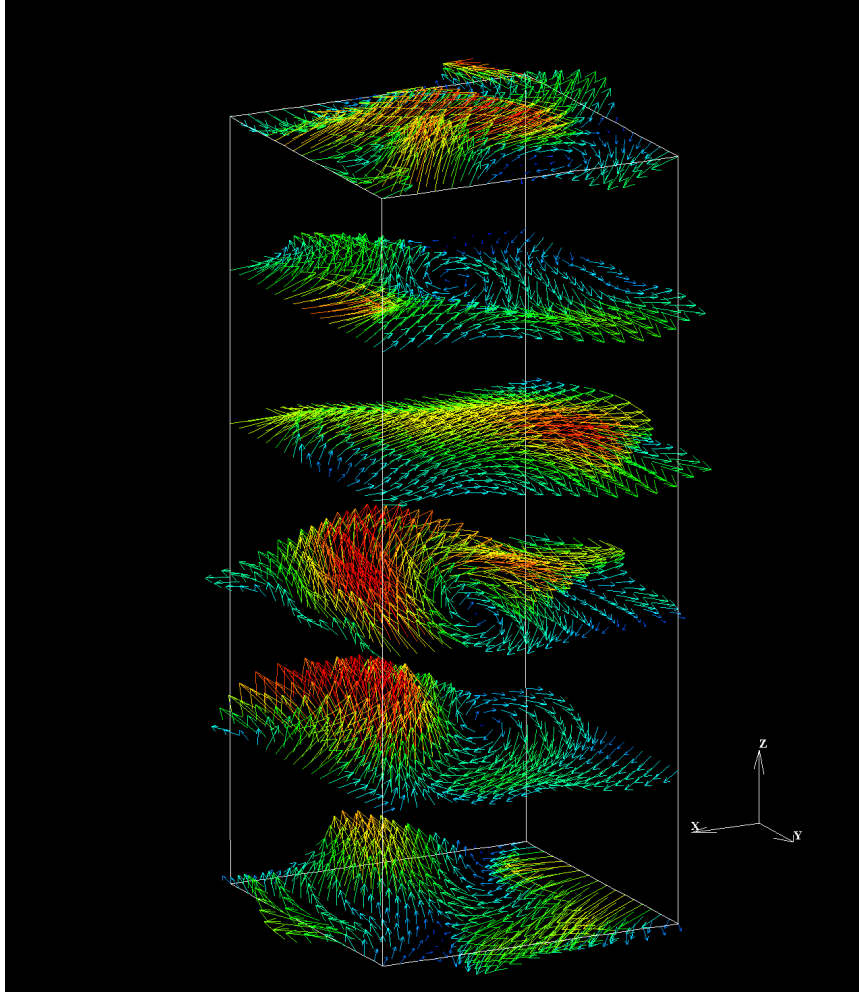


Fig. 9. Pseudo-3D vorticity vector distribution obtained by the time-resolved stereoscopic PIV in a turbulent swirling flow.

magnitude across the measurement plane is shaded and shown with velocity vector in the measurement plane. The velocity from behind the sheet to the front has positive value and is denoted by red color. As the measurement was conducted with 11.1kHz, flow maps with every $90\mu\text{s}$ were obtained. However, in Fig. 7, those with $180\mu\text{s}$ separation are presented to show the vortical motion well. From the sequential flow maps, it is clear that dynamics of vortical structures, which appear in turbulent swirling flows, are well represented by the time-resolved stereoscopic PIV system.

Figure 8 shows power spectrums of the three velocity components obtained by the time-resolved stereoscopic PIV in turbulent swirling flows. Energy spectrums of all velocity components show a distinct inertial subrange. As for the accuracy of out-of-plane velocity component (w), Lawson and Wu (1997) have shown that the accuracy of w is lesser than those of other components and is proportional to $1/\tan\theta$ and is inherent defect of the stereoscopic PIV. The energy spectrum of w obtained in the present study shows slightly larger values in high frequency region. Although the accuracy of out-of-plane velocity component is a little bit lower than other velocity components, this time-resolved stereoscopic PIV system provides temporal developments of three component velocities in a two-dimensional plane, and gives useful information for understandings the turbulent structures in detail. Figure 9 shows pseudo-3D vorticity vector distributions. In the present study, since the turbulent swirling flow is treated, mean azimuthal velocity exists. Therefore, pseudo-3D velocity field can be obtained approximately from the time-resolved stereoscopic PIV using Taylor's hypothesis. The z direction in Fig. 9 corresponds to the time evolution and vorticity vectors are visualized every $540\mu\text{s}$ (6 intervals). Figure 9 well represents dynamics of the eddy structure passing through the measurement plane.

4. SUMMARY

In this study, a time-resolved stereoscopic digital PIV system has been developed with high-repetition-rate Nd:YAG lasers for industrial processing and high-speed CMOS cameras. The developed system was applied to the velocity measurement of a turbulent jet and a swirl-stabilized combustor. It is shown that velocity measurement up to 26.7kHz is possible and the results represent dynamics of the turbulence structure very well. The time-resolved stereoscopic PIV can provide energy spectrums of three velocity components as well as the time-averaged feature of the turbulent flows with high accuracy. This system is potentially applicable from several hundred Hz to several tens kHz, and would contribute to developments of the turbulence research in the near future.

ACKNOWLEDGMENTS

This work is partially supported by Grant-in-Aid for Scientific Research (A) of Japan Society for the Promotion of Science and by the collaborative research project on "Smart Control of Turbulence: A Millennium Challenge for Innovative Thermal and Fluids Systems" of the Ministry of Education, Culture, Sports, Science and Technology, Japan.

REFERENCES

- Adrian R. J. (1991). "Particle-imaging techniques for experimental fluid mechanics", *Annual Review of Fluid Mechanics*, 23, pp. 261-304.
- Arroyo M. P. and Greated C. A. (1991). "Stereoscopic particle image velocimetry", *Measurement Science and Technology*, 2, pp. 1181-1186.
- Bruecker C. (1996). "3D PIV via spatial correlation in a color-coded light sheet", *Experiments in Fluids*, 21, pp. 312-314.
- Coupland J. M. and Halliwell N. A. (1992) "Particle image velocimetry: three-dimensional fluid velocity measurements using holographic recording and optical correlation", *Applied Optics*, 31, pp.1005-1007.
- Dudderrar T. D. and Simpkins P. G. (1977). "Laser speckle photography in a fluid medium", *Nature*, 270, pp. 45-47.
- Gaydon M., Raffel M., Willert C., Rosengarten M. and Kompenhans J. (1997). "Hybrid stereoscopic particle image velocimetry", *Experiments in Fluids*, 23, pp.331-334.
- Grant I., Fu S., Pan X. and Wang X. (1995). "The application of an in-line, stereoscopic, PIV System to 3-component velocity measurements", *Experiments in Fluids*, 21, pp.214-221.
- Ibsen C. H., Onofri F., Solberg T., Hjertager B. H. and Tadrst L. (2003). "Improved particle image velocimetry measurements in gas-particle flows with a dense wall layer", *Measurement Science and Technology*, 14, pp.N9-N12.
- Keane R. D. and Adrian R. J. (1990). "Optimization of particle image velocimeters. Part I: Double pulsed systems", *Measurement Science and Technology*, 1, pp.1202-1215.
- Kumar S. and Banerjee S. (1998). "Development and application of a hierarchical system for digital particle image velocimetry to free-surface turbulence", *Physics of Fluids*, 10, pp. 160-177.
- Lawson N. J. and Wu J. (1997). "Three-dimensional particle image velocimetry: Experimental error analysis of a angular stereoscopic system", *Measurement Science and Technology*, 8, pp. 1455-1464.
- Mao Z. Q., Halliwell N. A. and Coupland J. M. (1993). "Particle image velocimetry: high-speed transparency scanning and correlation-peak location in optical processing system", *Applied Optics*, 32, pp. 5089-5091.
- Megerle M., Sick V. and Reuss D. L. (2002). "Measurement of digital particle image velocimetry precision using electro-optically created particle-image displacements", *Measurement Science and Technology*, 13, pp.997--1005.
- Panchapakesan N. R. and Lumley J. L. (1993). "Turbulence measurements in axisymmetric jets of air and helium. Part 1. Air jet", *Journal of Fluid Mechanics*, 246, pp.197-223.

- Prasad A. K. (2000). "Stereoscopic particle image velocimetry", *Experiments in Fluids*, 29, pp. 103-116.
- Raffel M., Gharib M., Ronneberger O. and Kompenhans J. (1995). "Feasibility study of three-dimensional PIV by correlating images of particles within parallel light sheets", *Experiments in Fluids*, 19, pp.69-77.
- Schlicke T. and Greated C. (2002) "Application of dual-plane particle image velocimetry to the measurement of breaking waves", *Measurement Science and Technology*, 13, pp.1990-1995.
- Schmidt M. and Loffler F. (1993). "Experimental investigations on two-phase flow past a sphere using digital particle-image-velocimetry", *Experiments in Fluids*, 14, pp. 296-304.
- Sharpe J. P. and Johnson K. M. (1992). "Particle image velocimetry fringe processing using an optically addressed spatial light modulator", *Applied Optics*, 31, pp.7399-7402.
- Sung J. and Yoo J. Y. (2003). "Near-wake vortex motions behind a cylinder at low Reynolds number", *Journal of Fluids and Structures*, 17, pp.261-274.
- Tanahashi M., Fukuchi Y., Fukuzato K. and Miyauchi T. (2002). "Turbulence measurements by high resolution time series particle image velocimetry", *Proceedings of Thermal Engineering Conference 2002*, pp.121-122(in Japanese).
- Tanahashi M., Fukuchi Y., Choi G.-M., Fukuzato K. and Miyauchi T. (2003). "High spatial resolution time-series PIV for turbulence measurement", *Turbulence, Heat and Mass Transfer 4*, pp. 245--252.
- Tanahashi M., Ootsu M., Fukushima M. and Miyauchi T. (2002). "Measurement of coherent fine scale eddies in turbulent mixing layer by DPIV", *Engineering Turbulence Modeling and Measurements 5.*, W. Rodi and N. Fueyo, Eds., Elsevier, pp.525-534.
- Tollmien W. (1926). "Berechnung turbulenter ausbreitungsvorgange", *Z.A.M.M.*, 6, pp.468-478.
- Upatnieks A., Driscoll J. F. and Ceccio S. L. (2002). "Cinema particle imaging velocimetry time history of the propagation velocity of the base of a lifted turbulent jet flame", *Proceedings of the Combustion Institute*, 29, pp.1897-1903.
- Vogel A. and Lauterborn W. (1998). "Time resolved particle image velocimetry", *Optics and Lasers in Engineering*, 9, 277-294.
- Westerweel J. and Nieuwstadt F. T. M. (1991). "Laser anemometry advances and applications", *ASME*, pp. 349-355.
- Westerweel J., Dabiri D. and Garib M., (1997). "The effect of a discrete window offset on the accuracy of cross-correlationanalysis of digital PIV recordings", *Experiments in Fluids*, 23, pp.20-28.
- Willert C. and Gharib M. (1991). "Digital particle image velocimetry", *Experiments in Fluids*, 10, pp. 181-193.
- Willert C. (1997). "Stereoscopic digital particle image velocimetry for application in wind tunnel flows", *Measurement Science and Technology*, 8, pp.1465-1479.
- Wynanski I. and Fiedler H. (1969). "Some measurements in the self-preserving jet", *Journal of Fluid Mechanics*, 38, pp. 577-612.
- Zang W. and Prasad A. K. (1997). "Performance evaluation of a scheinflug stereocamera for particle image velocimetry", *Applied Optics*, 36, pp.8738-8744.